ICES REPORT 16-09

April 2016

Initialization of phase-field fracture propagation in porous media using probability maps of fracture networks

by

Sanghyun Lee, Mary F. Wheeler, Thomas Wick, and Sanjay Srinivasan

The Institute for Computational Engineering and Sciences
The University of Texas at Austin
Austin, Texas 78712

Reference: Sanghyun Lee, Mary F. Wheeler, Thomas Wick, and Sanjay Srinivasan , "Initialization of phase-field fracture propagation in porous media using probability maps of fracture networks," ICES REPORT 16-09, The Institute for Computational Engineering and Sciences, The University of Texas at Austin, April 2016.

Initialization of phase-field fracture propagation in porous media using probability maps of fracture networks

Sanghyun Lee[a], Mary F. Wheeler[a,*], Thomas Wick[b], Sanjay Srinivasan[c]

[a] *The Institute for Computational Engineering and Sciences, The University of Texas at Austin, Austin, Texas 78712, USA*
[b] *RICAM, Austrian Academy of Sciences Altenberger Str. 69 4040 Linz, Austria*
[c] *John and Willie Leone Family Department of Energy and Mineral Engineering, The Pennsylvania State University, University Park, Pennsylvania 16802, USA*

Abstract

It is well known in the geophysical community that surface deflection information/micro-seismic data are considered to be one of the best diagnostics for revealing the volume of rock fracture. However, the in-exactness of the data representing the deformation induced to calibrate and represent complex fracture networks created and connected during hydraulic fracturing presents a challenge. In this paper, we propose a technique that implements a phase field approach to propagate fractures and their interaction with existing fracture networks using surface deflection data. The latter one provides a probability map of fractures in a heterogeneous reservoir. These data are used to initialize both the location of the fractures and the phase-field function. In addition, this approach has the potential for optimizing well placement/spacing for fluid-filled fracture propagation for oil and gas production and or carbon sequestration and utilization. Using prototype models based on realistic field data, we demonstrate the effects of interactions between existing and propagating fractures in terms of several numerical simulations with different probability thresholds, locations, and numbers of fractures. Our results indicate that propagating fractures interact in a complex manner with the existing fracture network. The modeled propagation of hydraulic fractures is sensitive to the threshold employed within the phase field approach for delineating fractures.

Keywords: Hydraulic fracturing, probability map, phase-field fracture formulation

1. Introduction

The injection of large volumes of fluids in to the subsurface such as during geologic sequestration of CO_2 or during hydraulic fracturing operations can cause geomechanical deformation of the rock mass in the vicinity of the well. This in turn can trigger shear-slip events along existing faults and fractures or can manifest in the form of surface deflection that can be recorded by satellite-based remote sensing equipment. Because the network of natural fractures has an important effect on these types of responses either as locations along which micro-seismic slip events [3] or by acting as conduits for fluid flow that in turn determine the direction and extent of surface deflection, it is conjectured that inverse modeling of these responses can yield better characterization of the natural fracture network in the vicinity of wells. This notion is explored in the following study.

Figure 1 shows a map of surface deflection recorded using remote sensing sensors on board an InSAR (Interferometric Synthetic Aperture Radar) satellite. This data was collected for the In Salah Gas Joint Venture in Algeria which is an ongoing CO_2 storage project operational since August 2004. The Krechba field is part of the In Salah gas field

*Corresponding author
Email addresses: shlee@ices.utexas.edu (Sanghyun Lee), mfw@ices.utexas.edu (Mary F. Wheeler), thomas.wick@ricam.oeaw.ac.at (Thomas Wick), sanjays@psu.edu (Sanjay Srinivasan)

[1] This work by S. Lee, M. F. Wheeler, and S. Srinivasan was supported as part of the CFSES, an Energy Frontier Research Center funded by the U.S. Department of Energy, Office of Science, Basic Energy Sciences under Award #DE-SC0001114.

[2] T. Wick would like to thank the JT Oden Program of the *Institute for Computational Engineering and Science (ICES)* and the Center for Subsurface Modeling (CSM), UT Austin for hospitality during his visit in August 2015.

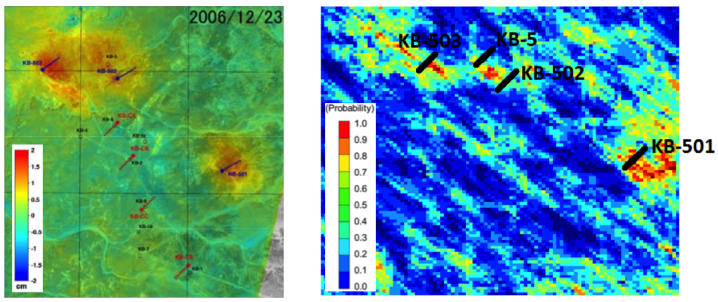

Figure 1: Left: Surface deformation map at the site in December 2006 [23]. Right: Posterior probability of fractures based on the ensemble mean of the models in the selected cluster. The location of the wells is also indicated in the figure.

development, and is currently the largest onshore CO_2 storage site in the world [11]. At Krechba, CO_2 from several gas fields is removed from the production stream and injected into the deep saline carboniferous formation away from the producers. The large volume of injected CO_2 causes ground upheaval that is shown in Figure 1.

Various methods deriving fracture networks from micro-seismic data as a framework for modeling reservoir performance have been suggested in order to connect a given natural fracture network with propagating hydraulic fractures [30]; here we employ a phase-field approach. Presently, this technique for fracture propagation is subject of intensive research in both mathematical theory and applications. Based on variational principles, they provide an elegant way to approximate lower-dimensional surfaces and discontinuities. Rewriting Griffith's model [8] for brittle fracture in terms of a variational formulation was first accomplished by [6, 7]. In [16, 15], the authors refined modeling and material law assumptions to formulate an incremental thermodynamically consistent phase-field model for fracture propagation. Numerous examples and benchmarks have been studied in [16, 15, 4, 5, 10, 25, 1]. Recent modeling and numerical studies of hydraulic fracturing in porous media and other multi-physics applications including thermo-elastic-plastic solids have been considered in [20, 19, 28, 18, 17]. Important computations of fluid-filled fractures in porous media with related findings using extended finite elements have been reported, for example, in [26, 27].

The goal of this paper is to detect given (natural) fractures with a probability map that can be obtained from microseismic or InSAR data. Then, these initial data are used to build the initial phase-field solution for our fluid-filled fracture models [14, 13, 19, 21]. More precisely, a probability map reflects the regions in which the stress conditions are such that there is a high probability of propagating fractures and so, this becomes the basis for our treating the probability map as the phase-field function for the fracture propagation modeling.

2. Construction of probability map and phase-field initialization

The procedure to constrain a set of models for the natural fracture network to the surface deflection information starts with an initial suite of models that reflects the prior uncertainty in describing the network. Models in this initial set reflect fractures of arbitrary orientation and possibly extent as shown in Figure 2. Flow and geomechanics responses of the prior models were obtained using a coupled proxy developed in [22]. The proxy utilizes a particle tracking simulation to model the flow of CO_2 in the prior models and couples that response to a simplified geomechanical scheme for computing the surface deflection corresponding to the injection of large volumes of CO_2 into the model. The simplified proxy allows evaluating the response of a large suite of models efficiently. The dissimilarity between pairs of models in the prior set are computed. These dissimilarities are subsequently transformed to a metric space using multidimensional scaling (MDS) [12]. Figure 3 depicts the cluster of responses when projected in the metric space obtained by MDS. In this figure, models (depicted by points) that are close to each other exhibit similar dynamic responses. Cluster analysis can be performed and the grouping of models is also shown in Figure 3 in the form of clusters of different colors. The optimal number of clusters is selected on the basis of a silhouette measure [24] that is a ratio of the inter-cluster to the intra-cluster distances. Coupled geomechanical-flow simulation was performed for one representative member of each cluster. These simulations solve the physical equations governing the flow and

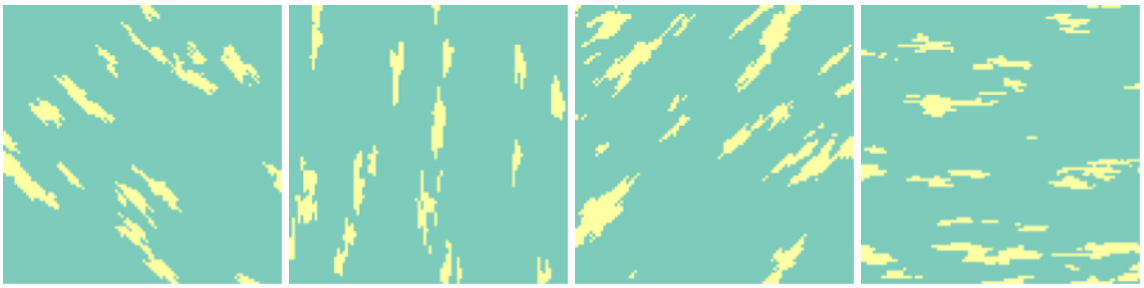

Figure 2: Initial set of fracture models generated using geostatistical schemes.

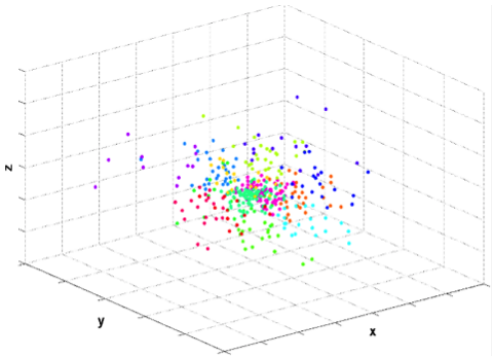

Figure 3: Results of MDS and clustering of 400 model observations in three-dimensional space.

transport of CO_2 and the mechanical equations describing the deformation of the reservoir. A finite difference scheme utilizing a flexible grid is utilized for discretizing and solving the governing equations [9]. The representative model is taken to be the model closest to the medoid of each cluster. The responses obtained for the representative models were compared to the observed surface deflection observed in Figure 1. The similarity between the simulated and observed responses was computed as the square difference between the grid cell surface deflection values. The cluster with the closest response to the observation was retained. Some of the models in the selected cluster are shown in 4. More details regarding this model selection process utilizing the surface deflection information can be found in [22]. The model selection process yields a suite of models that have binary values indicating the presence or absence of

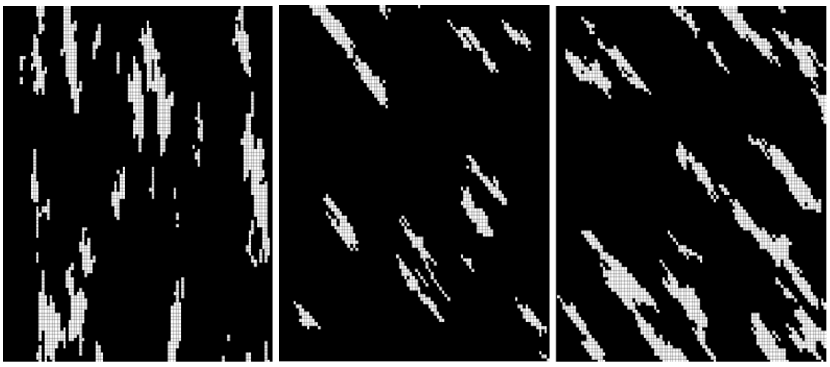

Figure 4: Sample models from the selected cluster.

fracture at a location. Denoting the presence or absence of a fracture at a location ξ in the reservoir model l by the indicator $I^l(\xi)$, the ensemble average computed over the suite of models in the selected cluster yields the probability

that there is a fracture at that location in the reservoir

$$E\{I(\xi)\} = \frac{1}{L}\sum_{l=1}^{L} I^l(\xi) = \text{Prob}\{\xi \in \text{fracture}\}.$$

Repeating the ensemble averaging process at each location in the reservoir model, we obtain the probability map shown in Figure 1. This probability map quantifies the uncertainty in delineating the fracture distribution based on the available surface deflection data. The use of this map for phase field modeling is discussed next.

Figure 1 shows the probability map for the presence of a fracture derived from the posterior ensemble from model selection. The probability value $m \in [0, 1]$ indicates 0 for zero probability of fracture and 1 for 100% of fracture. In the poroelastic domain Λ, a phase field function $\varphi(\cdot, t) : \Lambda \times [0, T] \to [0, 1]$ is defined. For $\varphi(\cdot, t) = 0$, we denote a crack region and $\varphi(\cdot, t) = 1$ is the unbroken material. The intermediate values constitute a so-called transition zone that is dependent on a regularization (or length-scale) parameter ε. In particular, ε is the thickness of the transition zone. The probability values are used as follows to initialize the phase-field solution:

$$\varphi(\cdot, 0) = \begin{cases} 0, & 1 - m < m_L \\ (1 - m), & m_U < 1 - m < m_L \\ 1, & 1 - m > m_U \end{cases} \tag{1}$$

Here, m_L and m_U are lower and upper thresholds. Sensitivity to different values of m_L and m_U are explored in the Section 4 of the paper.

3. Fluid-filled phase-field fracture modeling and discretization

In this section, we describe the governing equations for displacements, phase-field and pressure. We assume the input of a single phase fluid and linear elastic geo-mechanical properties.

3.1. Phase-field fracture modeling

We adopt a phase-field approach in terms of the Euler-Lagrange weak formulation for hydraulic fractures that has been derived in [21, 20]. Let the pressure $p(\cdot, t) : \Lambda \times [0, T] \to \mathbb{R}$ be given. The unknown solution variables are vector-valued displacements $\mathbf{u}(\cdot, t) : \Lambda \times [0, T] \to \mathbb{R}^d$ and a smoothed indicator phase-field function φ. Due to the crack irreversibility condition, $\varphi \leq \varphi^{old}$, the resulting system is a variational inequality.

Let $V := H_0^1(\Lambda), W := H^1(\Lambda)$ and $W^{in}_{\varphi^{old}} := \{w \in H^1(\Lambda) | \, w \leq \varphi^{old} \leq 1 \text{ a.e. on } \Lambda\}$ be the function spaces for the displacements and the phase field, respectively. The variational inequality system for hydraulic fractures then reads as:

Formulation 1. *For given p, find* $(\mathbf{u}, \varphi) \in V \times W^{in}_{\varphi^{old}}$ *such that*

$$\int_\Lambda \left((1-\kappa)\varphi^2 + \kappa\right) \boldsymbol{\sigma}(\mathbf{u}), \mathbf{e}(\mathbf{w})\Big) \, d\mathbf{x} - \int_\Lambda (\alpha - 1)(\varphi^2 p, div\ \mathbf{w}) \, d\mathbf{x} = 0 \quad \forall \mathbf{w} \in V, \tag{2}$$

$$\int_\Lambda (1-\kappa)(\varphi\ \boldsymbol{\sigma}(\mathbf{u}) : \mathbf{e}(\mathbf{u}), \psi - \varphi) d\mathbf{x} - \int_\Lambda 2(\alpha - 1)(\varphi\ p\ div\ \mathbf{u}, \psi - \varphi) d\mathbf{x} + \int_\Lambda G_c\Big(-\frac{1}{\varepsilon}(1-\varphi, \psi - \varphi) + \varepsilon(\nabla\varphi, \nabla\psi - \varphi)\Big) d\mathbf{x} \geq 0$$
$$\forall\ \psi \in W \cap L^\infty(\Lambda), \tag{3}$$

where, $\boldsymbol{\sigma} = \boldsymbol{\sigma}(\mathbf{u})$ *is the stress tensor,*

$$\boldsymbol{\sigma} := \boldsymbol{\sigma}(\mathbf{u}) = 2\mu\mathbf{e}(\mathbf{u}) + \lambda\ tr(\mathbf{e}(\mathbf{u}))\mathbf{I},$$

and $\mathbf{e}(\mathbf{u})$ *is the symmetric (linearized) strain tensor defined as* $\mathbf{e}(\mathbf{u}) := \frac{1}{2}\left(\nabla\mathbf{u} + \nabla\mathbf{u}^T\right)$. *Here* μ *and* λ *are material parameters,* $\mathbf{I}$ *is the identity matrix,* $G_c > 0$ *is the energy release rate,* ε *is the previously mentioned crack surface regularization parameter, and finally* κ *is a positive regularization parameter for the elastic energy, with* $\kappa \ll \varepsilon$. *Finally, the time* $0 \leq t \leq T$ *enters through time-dependent coefficients and right-hand side data.*

3.2. A pressure diffraction system for modeling reservoir and fracture flow

In order to formulate the flow equations in the porous media zone and the fracture, respectively, we employ the phase field function as an indicator function [19, 14]. Thus, the flow pressure equations can be separated for the fracture ($p_F(\cdot,t) : \Lambda \times [0,T] \to \mathbb{R}$) and the reservoir ($p_R(\cdot,t) : \Lambda \times [0,T] \to \mathbb{R}$) sub-domains respectively. The resulting system leads to a pressure diffraction problem.

We denote by $\Omega_F(t)$ and $\Omega_R(t)$ the open subsets of the space-time domain $\Lambda \times [0,T]$. $\Omega_R(t)$ is filled with the unbroken material (reservoir domain) and the fracture is approximated by a volume domain $\Omega_F(t)$, where we initialize $\Omega_F(0)$ by (1), which is defined by the probability map. Additional fractures can be introduced through well models. We set $\Gamma(t) := \bar{\Omega}_F(t) \cap \bar{\Omega}_R(t)$.

To derive the flow pressure equations for each sub-domains, first we consider the two separate mass continuity equations for the fluid in the reservoir and the fracture, which we can rewrite as

$$\partial_t(\rho\phi^\star) + \nabla \cdot (\rho \mathbf{v}) = q \quad \text{in} \quad \Lambda \times (0,T]. \tag{4}$$

Here $\phi^\star := \varphi\phi_R^\star + (1-\varphi)\phi_F^\star$ is the fluid fraction, where $\phi_R^\star$ and $\phi_F^\star$ are the reservoir and fracture fluid fraction respectively. We assume $\phi_F^\star = 1$ (since the porosity of the fracture is one), and the reservoir fluid fraction is given as $\phi_R^\star = \phi_0^\star + \alpha\nabla\cdot\mathbf{u} + \frac{1}{M}(p - p_0)$, where α is Biot's coefficient, and p_0 is an initial pressure value. Next, we describe the flow $\mathbf{v} := \varphi\mathbf{v}_R + (1-\varphi)\mathbf{v}_F$, given by Darcy's law

$$\mathbf{v}_j = -\frac{K_j}{\eta_j}(\nabla p_j - \rho_j \mathbf{g}), \tag{5}$$

for the fracture ($j = F$) and for the reservoir ($j = R$), respectively, with given gravity $\mathbf{g}$. We assume the fluid in the reservoir and the fracture is slightly compressible, thus we define the fluid density $\rho := \varphi\rho_R + (1-\varphi)\rho_F$ as

$$\rho_j := \rho_j^0 \exp(c_j(p_j - p_j^0)) \approx \rho_j^0[1 + c_j(p_j - p_j^0)], \tag{6}$$

where ρ_j^0 is the reference density and c_j is the fluid compressibility. In addition, q is a source/sink term which can also include the leak-off [19]. Following the general reservoir approximation with the assumption that c_R and c_F are small enough, we use $\rho_R = \rho_R^0$ and $\rho_F = \rho_F^0$.

Taking the mass conservation equation (4) for both the reservoir and the fracture, and then formulating them in terms of a diffraction problem [19] and integration by parts, we obtain:

Formulation 2. *For given initial conditions $p(\cdot,0)$, $\mathbf{u}(\cdot,0)$, and $\varphi(\cdot,0)$, find $\{p_R, p_F\}$ in terms of a global pressure $p \in H^1(\Lambda)$ for all times t such that*

$$\begin{aligned}
&\int_\Lambda \varphi\Big(\rho_R^0\partial_t(\frac{1}{M}p_R + \alpha\nabla\cdot\mathbf{u})\Big)\omega d\mathbf{x} + \int_\Lambda \Big(\frac{K_R\rho_R^0}{\eta_R}(\nabla p_R - \rho_R^0\mathbf{g})\Big) : \nabla\omega d\mathbf{x} = \int_\Lambda \varphi q_R\omega d\mathbf{x},\\
&\int_\Lambda (1-\varphi)\Big(\rho_F^0 c_F\partial_t p_F\Big)\omega d\mathbf{x} + \int_\Lambda \Big(\frac{K_F\rho_F^0}{\eta_F}(\nabla p_F - \rho_F^0\mathbf{g})\Big) : \nabla\omega d\mathbf{x} = \int_\Lambda (1-\varphi)q_F\omega d\mathbf{x}, \forall\omega \in H^1(\Lambda).
\end{aligned} \tag{7}$$

where $w(\mathbf{u}) = [\mathbf{u}\cdot\mathbf{n}]$ (where $\mathbf{n}$ is the unit normal vector) denotes the aperture of the fracture. The jump $[\cdot]$ of normal displacements is computed point-wise at each node. This approximation is valid for symmetric fractures but does also yield the correct order for non-symmetric and non-aligned fracture networks. However, a systematic justification is not yet available in existing literature.

For the fracture flow, we adopt a three-dimensional lubrication equation and an anisotropic fracture permeability K_F has been derived in [19]. This absolute fracture permeability leads to an effective permeability K_{eff} in the phase-field transition zone. As (briefly) discussed in [14], K_{eff} is clearly sensitive to the transition zone and related stability is ongoing work.

The interface conditions on $\Gamma \times (0,T]$ are implicitly contained in Formulation 2 and are given by,

$$p_R = p_F, \quad \mathbf{v}_F\cdot\mathbf{n} = \mathbf{v}_R\cdot\mathbf{n}. \tag{8}$$

3.3. Adaptive discretization and numerical solution

The adaptive discretization and coupling of displacement, phase-field and pressure diffraction equations are based on the techniques described in [10, 14, 19]. Spatial discretization is based on Galerkin finite elements whereas time discretization is performed by a A-stable backward Euler time stepping scheme. Nonlinear problems are solved with Newton's method and analytical evaluation of the Jacobian. The linear equations are solved with parallel MPI-based iterative solvers (GMRES) with block-diagonal pre-conditioning. The programming code has been discussed in [14, 29] based on the framework [10] using deal.II [2].

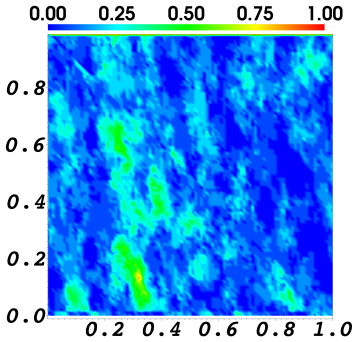

Figure 5: Given probability map values. Here 0 corresponds to zero fracture probability and 1 to a fracture.

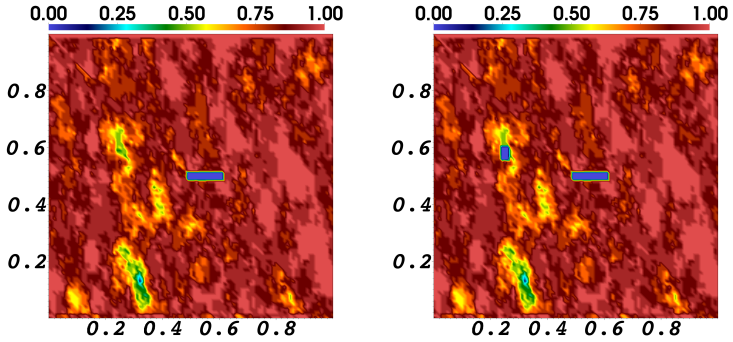

Figure 6: Left: Initial phase-field solution by combining the probability data including their thresholds with the two hydraulic fractures (Case 2). Right: Initial phase-field solution by combining the probability data including their thresholds with two hydraulic fractures (Case 4).

4. Numerical tests

In this final section, we present numerical results that show how to translate the probability map into an initial phase-field function. With that we then focus on the sensitivity of crack propagation depending on the interpretation of the probability map and on the number of initial fractures. Our objective is to observe certain goal functionals such as the fracture patterns and joining with natural fractures while injecting a fluid into hydraulic cracks.

Configuration. The domain is localized to $\Lambda = (1\,\mathrm{m}, 1\,\mathrm{m})^2$. The given probability map relates to each grid cell an initial fracture probability. These data transform directly to an initial phase-field solution. As explained earlier we use a lower threshold m_L to indicate fractured regions and an upper threshold m_U to indicate intact or non-fractured domains. In order to observe sensitivity of these thresholds on fracture propagation, its path, and the maximum pressure evolution, we choose different thresholds values. In Case 1 and 2, we set $m_L = 0.5$ and $m_U = 0.8$; and for

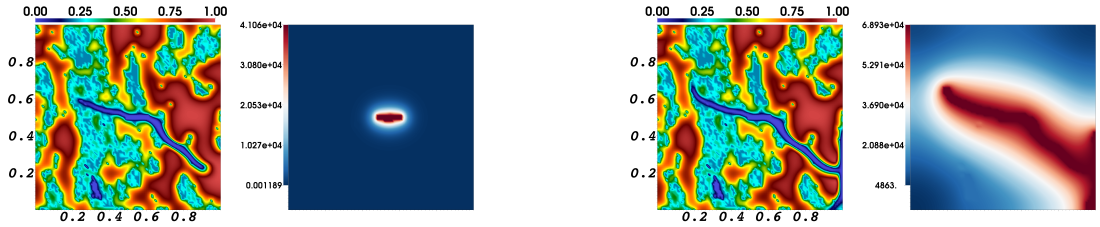

(a) $T = 1s$ (b) $T = 50s$

Figure 7: Case 1. For each time (a) $T = 1s$ and (b) $T = 50s$, we plot the phase field value (left) and the corresponding pressure value (right). For the phase field, blue indicates $\varphi = 0$ and red indicates $\varphi = 1$. We observe a single hydraulic fracture propagating and interacting with initial fractures.

Case 3 and 4 we set $m_L = 0.3$ and $m_U = 0.9$. These fractures are interpreted as natural fractures. To observe fracture interaction, we initiate hydraulic fractures (one fracture for Case 1 and 3; and two fractures for Case 2 and 4) by well injections. Due to the fluid injection, the pressure increases and finally results in fracture propagation.

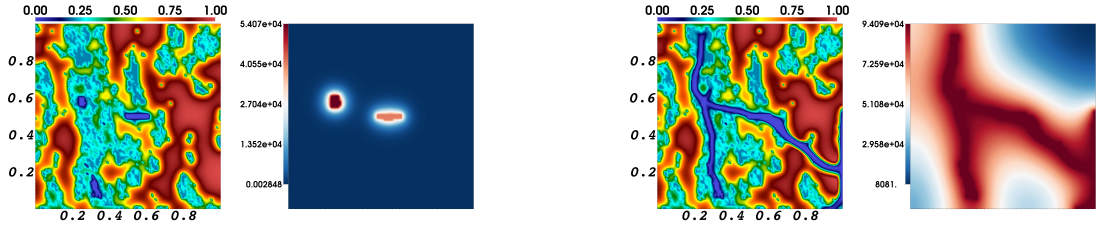

(a) $T = 1s$ (b) $T = 50s$

Figure 8: Case 2. In extension to Case 1, we prescribe two hydraulic fractures. As before, the fracture pattern (including branching and joining with natural fractures) and the corresponding pressure distribution are shown.

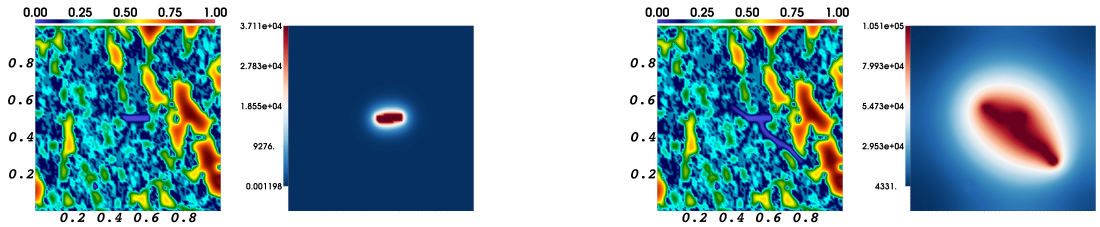

(a) $T = 1s$ (b) $T = 50s$

Figure 9: Case 3. Compared to Case 1 (Figure 7), different values of thresholds m_U and m_L give both different initial fracture patterns and propagations.

Boundary and initial conditions On the boundary $\partial\Lambda$ we prescribe homogeneous Dirichlet conditions for the displacements. For the phase-field we employ homogeneous Neumann conditions (traction-free) as usual. For the pressure, no flow conditions (realized as homogeneous Neumann conditions) are given. The hydraulic (fluid-filled) fractures are prescribed as an initial condition of the phase-field variable. In these fractures regions the initial pressure is set to 10^2 Pa. A point source injection is modeled as $q_f = p_{pb} \frac{d}{\pi} exp(-d*(\mathbf{x}-\mathbf{x}_0)^2)$ where $d = 10000$, $p_{bp} = 2.0\times10^{-5}$ with $\mathbf{x}_0 = (0.55, 0.5)$ (Case 1 and 3) and $\mathbf{x}_0 = (0.25, 0.58)$ (Case 2 and 4).

Parameters. As numerical parameters we set $\kappa = 10^{-12}$, $h = 0.14\,\mathrm{m}$ $\varepsilon = 0.028 = 2h$, $T = 50\,\mathrm{s}$, and $\alpha = 1.0$. The time step size is $\delta t = 1\,\mathrm{s}$. Other physical parameters are given as $K_R = 10^{-14}$, $c_R = c_F = 10^{-11}\,\mathrm{Pa}^{-1}$, $\eta_R = \eta_F = 10^{-3}\,\mathrm{kg\,m\,s}^{-1}$, $E = 10^8\,\mathrm{Pa}$, $\nu_s = 0.2$, and $G_c = 1\,\mathrm{J/m}^2$.

Quantities of interest. For each case, we observe the maximum pressure, the pressure distribution, fracture propagation and the fracture pattern. *Discussion of our findings.* In Figure 7 - Figure 11, our results are displayed. We observe that fracture propagation and its path and pattern are sensitive to the threshold values and the number of initial hydraulic fractures. Moreover, the maximal pressure (see Figure 11) inside the fracture is sensitive to the initial data.

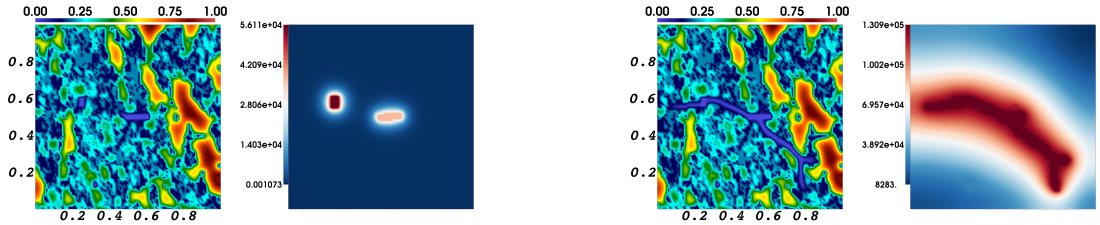

(a) $T = 1s$ (b) $T = 50s$

Figure 10: Case 4. We use the same thresholds m_U and m_L as in Case 3 but prescribe two hydraulic fractures (as in Case 2). It can be observed that the two fractures join and split.

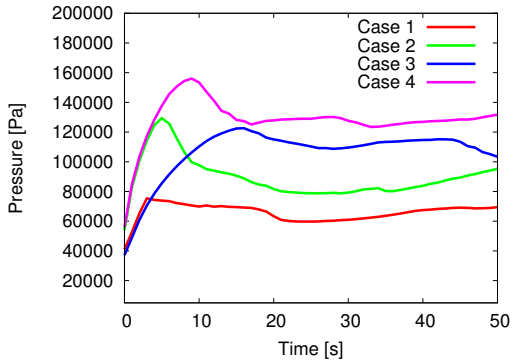

Figure 11: Maximum pressure evolution at the injection point over time. In all cases, we first observe a pressure build-up that is followed by a pressure decrease when the fracture(s) are propagating. Moreover, there is a second significant decrease when the two fractures join in Case 2 and 4.

Conclusions

In this work, we propose the coupling of probability maps from satellite or microseismic data with phase field functions for describing the location and propagation of fractures in porous media. Our preliminary results demonstrate that fracture propagation and its path and pattern, as well as the maximal pressure inside the fracture are all sensitive to the interpretation of the data and the number of initial fractures. Based on our findings we feel this approach has the potential in addressing the complex interactions of fracture propagation. The probability model used as an input to the deterministic phase field approach indicates that there is uncertainty associated with exactly predicting the location of a fracture. A refinement to our approach would be to draw realizations of the fracture from the calculated probability values and use the drawn fracture to define the deformed region for phase field modeling. Different realizations of the fracture would then yield different phase field results thereby quantifying the uncertainty in fracture propagation. Complete studies for validations can be achieved in future work once more experimental data are given and the model framework is extended to include seismic wave propagation.

References

[1] M. Ambati, T. Gerasimov, and L. De Lorenzis. Phase-field modeling of ductile fracture. *Computational Mechanics*, pages 1–24, 2015. ISSN 0178-7675.

[2] W. Bangerth, R. Hartmann, and G. Kanschat. deal.II – a general purpose object oriented finite element library. *ACM Trans. Math. Softw.*, 33 (4):24/1–24/27, 2007.

[3] S. P. Bordas, editor. *Advances in Applied Mechanics*, volume 47 of *Advances in Applied Mechanics*. Academic Press, 2014.

[4] M. J. Borden, C. V. Verhoosel, M. A. Scott, T. J. R. Hughes, and C. M. Landis. A phase-field description of dynamic brittle fracture. *Comput. Meth. Appl. Mech. Engrg.*, 217:77–95, 2012.

[5] M. J. Borden, T. J. Hughes, C. M. Landis, and C. V. Verhoosel. A higher-order phase-field model for brittle fracture: Formulation and analysis within the isogeometric analysis framework. *Comput. Methods Appl. Mech. Engrg.*, 273:100–118, 2014.

[6] B. Bourdin, G. Francfort, and J.-J. Marigo. Numerical experiments in revisited brittle fracture. *J. Mech. Phys. Solids*, 48(4):797–826, 2000.

[7] G. Francfort and J.-J. Marigo. Revisiting brittle fracture as an energy minimization problem. *J. Mech. Phys. Solids*, 46(8):1319–1342, 1998.

[8] A. Griffith. The phenomena of rupture and flow in solids. *Philos. Trans. R. Soc. Lond.*, 221:163–198, 1921.

[9] C. M. Group. *CMG - GEM User Manual*, 2011.

[10] T. Heister, M. F. Wheeler, and T. Wick. A primal-dual active set method and predictor-corrector mesh adaptivity for computing fracture propagation using a phase-field approach. *Comput. Methods Appl. Mech. Engrg.*, 290:466–495, 2015.

[11] M. Iding and P. Ringrose. Evaluating the impact of fractures on the long-term performance of the In Salah CO_2 storage site. *Energy Procedia*, 1(1):2021–2028, 2009.

[12] J. B. Kruskal. Nonmetric multidimensional scaling: A numerical method. *Psychometrika*, 29(2):115–129, 1964.

[13] S. Lee, A. Mikelić, M. F. Wheeler, and T. Wick. Phase-field modeling of proppant-filled fractures in a poroelastic medium. *Comput. Meth. Appl. Mech. Engrg.* doi: http://dx.doi.org/10.1016/j.cma.2016.02.008.

[14] S. Lee, M. F. Wheeler, and T. Wick. Pressure and fluid-driven fracture propagation in porous media using an adaptive finite element phase field model. *Comput. Meth. Appl. Mech. Engrg.*, 305:111 – 132, 2016. doi: http://dx.doi.org/10.1016/j.cma.2016.02.037.

[15] C. Miehe, M. Hofacker, and F. Welschinger. A phase field model for rate-independent crack propagation: Robust algorithmic implementation based on operator splits. *Comput. Meth. Appl. Mech. Engrg.*, 199:2765–2778, 2010.

[16] C. Miehe, F. Welschinger, and M. Hofacker. Thermodynamically consistent phase-field models of fracture: variational principles and multi-field fe implementations. *International Journal of Numerical Methods in Engineering*, 83:1273–1311, 2010.

[17] C. Miehe, M. Hofacker, L.-M. Schaenzel, and F. Aldakheel. Phase field modeling of fracture in multi-physics problems. part ii. coupled brittle-to-ductile failure criteria and crack propagation in thermo-elasticplastic solids. *Comput. Methods Appl. Mech. Engrg.*, 294:486 – 522, 2015.

[18] C. Miehe, L.-M. Schaenzel, and H. Ulmer. Phase field modeling of fracture in multi-physics problems. part i. balance of crack surface and failure criteria for brittle crack propagation in thermo-elastic solids. *Comput. Methods Appl. Mech. Engrg.*, 294:449 – 485, 2015.

[19] A. Mikelić, M. F. Wheeler, and T. Wick. A phase-field method for propagating fluid-filled fractures coupled to a surrounding porous medium. *SIAM Multiscale Model. Simul.*, 13(1):367–398, 2015.

[20] A. Mikelić, M. F. Wheeler, and T. Wick. A quasi-static phase-field approach to pressurized fractures. *Nonlinearity*, 28(5):1371–1399, 2015.

[21] A. Mikelić, M. F. Wheeler, and T. Wick. Phase-field modeling of a fluid-driven fracture in a poroelastic medium. *Computational Geosciences*, 19(6):1171–1195, 2015.

[22] A. Nwachukwu. Model selection for CO_2 sequestration using surface deflection and injection data. Master's thesis, The University of Texas at Austin, 2015.

[23] T. Onuma, K. Okada, S. Ohkawa, et al. Surface heave detection related with CO_2 injection by DInSAR at In Salah, Algeria. In *International Petroleum Technology Conference*. International Petroleum Technology Conference, 2008.

[24] P. J. Rousseeuw. Silhouettes: A graphical aid to the interpretation and validation of cluster analysis. *Journal of Computational and Applied Mathematics*, 20:53 – 65, 1987.

[25] A. Schlüter, A. Willenbücher, C. Kuhn, and R. Müller. Phase field approximation of dynamic brittle fracture. *Comput. Mech.*, 54(5): 1141–1161, 2014. ISSN 0178-7675.

[26] B. A. Schrefler, S. Secchi, and L. Simoni. On adaptive refinement techniques in multi-field problems including cohesive fracture. *Comput. Meth. Appl. Mech. Engrg.*, 195:444–461, 2006.

[27] S. Secchi and B. Schrefler. Hydraulic fracturing and its peculiarities. *Asia Pacific Journal on Computational Engineering*, 1(1):8, 2014.

[28] M. Wheeler, T. Wick, and W. Wollner. An augmented-Lagangrian method for the phase-field approach for pressurized fractures. *Comp. Meth. Appl. Mech. Engrg.*, 271:69–85, 2014.

[29] T. Wick, S. Lee, and M. Wheeler. 3D phase-field for pressurized fracture propagation in heterogeneous media. *VI International Conference on Computational Methods for Coupled Problems in Science and Engineering 2015 Proceedings*, May 2015.

[30] X. Yu, J. T. Rutledge, S. W. Leaney, S. Maxwell, et al. Discrete-fracture-network generation from microseismic data by use of moment-tensor-and event-location-constrained hough transforms. *SPE Journal*, 2015.